ORIGINAL RESEARCH ARTICLE

Effect of Deformation on the Magnetic Properties of CrMnFeCoNi and CrMnFeCoNi-CN High-Entropy Alloys

L.G. TORRES-MEJÍA, C.A. PARRA-VARGAS, J. LENTZ, S. WEBER, and L. MUJICA-RONCERY

The magnetic behavior of two high-entropy alloys, CrMnFeCoNi and CrMnFeCoNi-CN, was investigated under varying degrees of deformation through uniaxial tensile tests. Microstructural, morphological, and crystalline structural analyses using XRD and SEM revealed a uniform and stable austenitic structure in all samples, with no presence of α'-martensite or ε-martensite phases. The main deformation mechanisms identified were twinning and slip dislocation for the CrMnFeCoNi-CN alloy, and slip dislocation for the CrMnFeCoNi alloy at room temperature. The alloys exhibited low magnetic moments attributed to magnetically frustrated configurations. At temperatures below 70 K, distinct magnetic states were observed ranging from paramagnetic to ferrimagnetic and spin-glass-like behavior. Antiferromagnetic interactions were confirmed by a negative paramagnetic Curie temperature for both alloys. The magnetization of the CrMnFeCoNi alloy increased with deformation, reflected in effective magnetic moments varying from 1.81 (0 pct) to 2.60 (20 pct) μB, while for the CrMnFeCoNi-CN alloy remained stable around 2.39 to 2.48 μB. The magnetization of the CrMnFeCoNi-CN alloy was found to be higher than that of the CrMnFeCoNi alloy, suggesting that the presence of C and N as alloying elements can enhance magnetization to some extent.

https://doi.org/10.1007/s11661-024-07514-5

I. INTRODUCTION

MULTICOMPONENT, compositionally complex alloys have been extensively studied due to their unique properties.[1–5] They disclose a variety of applications including electrocatalytic processes,[6–10] hydrogen storage,[11,12] structural components at low temperatures,[13] soft-magnetic materials,[13–15] among others. Some works have been addressed on the alloying of interstitial elements as C, N, and B as a promising way to improve mechanical properties of high-entropy alloys.[16,17] Extensive works have investigated mechanical properties of Cantor alloy and its derivatives.[16,18–25] While some studies have addressed the magnetic behavior of these alloys at low temperatures, the full understanding of the effect of parameters such as deformation on the magnetic properties is still incomplete. Cantor equimolar alloy has been identified as single fcc structure at room temperature with a favorable balance of work hardening rate (WHR), strength, ductility, and fracture toughness at low temperatures (down to cryogenic temperatures).[26] Gali and George[1] demonstrated for the first time that when temperature is lowered from 293 K to 77 K, the HEA CrMnFeCoNi shows an increase in the yield strength, ultimate tensile strength, and ductility. Simultaneously, Otto *et al.*[18] using transmission electron microscopy (TEM) come to the conclusion that the appearance of two deformation mechanisms at 77 K, namely dislocation slip and mechanical twinning, is related to the rise in ductility with the drop in temperature.

Cantor alloy exhibits paramagnetic properties at room temperature and competing magnetic interactions at lower temperatures.[27–30] Some other magnetic states as ferromagnetism,[27] ferrimagnetism,[31] and spin-glass-like behavior have been identified[31,32] for this alloy.

In spite of the fact that it is known that the 3d elements Cr, Mn, Fe, Co, and Ni have spontaneous magnetism even in the solid state, the spontaneous

L.G. TORRES-MEJÍA and L. MUJICA-RONCERY are with the Grupo de Investigación en Materiales Siderúrgicos, Universidad Pedagógica y Tecnológica de Colombia, 150003 Tunja, Boyacá, Colombia. Contact e-mails: lais.mujica@uptc.edu.co; laura.mejia01@uptc.edu.co C.A. PARRA-VARGAS is with the Grupo de Física de Materiales, Universidad Pedagógica y Tecnológica de Colombia, 150003 Tunja, Boyacá, Colombia. J. LENTZ and S. WEBER are with the Ruhr-Universität Bochum, Lehrstuhl Werkstofftechnik, 44801 Bochum, Germany.
Manuscript submitted January 4, 2024; accepted July 2, 2024.
Article published online July 24, 2024

magnetization of HEAs diminishes with an increase in the number of *d*- or *p*-elements that make up the alloy.[31] It has been shown that factors like alloying elements,[33–35] synthesis routes,[36] cooling rates,[35,37] grain size,[38] heat treatments, and plastic deformation[39,40] among others have an effect on the magnetic response of this type of alloys. For example, Babilas R. *et al*.[35] found that the introduction of Si and Cr in an AlFeCoNi alloy changes the value of the saturation of magnetization strongly. Saturation decreases with the increase of Cr and Si. Same effect was observed for the FeCoNi alloy.[41] It was discovered that the Mn content significantly influences the stabilization of antiferromagnetic configurations in alloys based on CrMnFeCoNi. These arrangements have a substantial effect on the SFE ultimately leading to a predominant deformation behavior.[33] Uporov *et al*. investigated how processing parameters influence phase evolution and their relationship with the magnetic properties of AlCoCrFeNi High-Entropy Alloys synthesized using the arc melting process.[42] The HEA was initially divided into three segments, each of which underwent distinct processing methods: vacuum suction casting, slow remelting in a resistance furnace, and annealing for varying durations at elevated temperatures. XRD analysis confirmed the presence of both fcc and bcc phases in all samples processed through the different methods. Specifically, the fcc phase predominated in samples subjected to long-duration annealing, while the bcc phase was dominant in as-cast, quenched, and remelted samples. Magnetic moment versus magnetic field (M–H) curves for all four samples at two distinct temperatures, 300 K and 4 K, showed the coercivity (Hc) values fell within the range of 60–160 Oe, indicating semi-hard magnetic behavior. Additionally, the saturation magnetization (Ms) ranged from 15 to 54 emu/g at room temperature. Notably, the reported Ms value was lower for the homogenized sample and higher for the non-homogenized samples. The authors suggested that the change in Ms may be attributed to the formation of fcc phase in the homogenized state. Foldeaki *et al*.[39] investigated the magnetic properties of three Cr–Mn austenitic stainless steels with deformations reaching up to 56 pct. Measurements on mechanically deformed specimens indicated a sensitivity of the molecular-field constants to the structure. This finding was explained cohesively by considering changes in lattice parameters. Transition temperatures can be affected by the deformation induced in the alloy, as demonstrated by Torres-Mejía *et al*.[40] In their study, the Néel temperature of a FeCrMn-based alloy exhibited an increase due to deformation, while a decrease in magnetization and magnetic susceptibility was reported for the deformed material.

Constituent elements, magnetic order may also have a significant impact on mechanical properties and phase stability.[43] Therefore, studying magnetism is appropriate in order to determine the magnetic ground state of fcc alloys and the impact of various conditions on their magnetic behavior. Enhancing our comprehension of the magnetic behavior of these alloys at low temperatures will pave the way for designing tailored alloys specifically suited for cryogenic engineering applications. These applications include the development of advanced materials for critical components such as superconducting magnets, cryogenic storage tanks, and low-temperature pipelines. Furthermore, the insights gained can also benefit the field of magnetic sensors, particularly those designed for precise and reliable operation in low-temperature environments. In this work, we performed a comprehensive analysis, combining deformation, temperature, and magnetic field effects, on the magnetization of both the Cantor CrMnFeCoNi and CrMnFeCoNi-CN alloys. This study is particularly significant as the influence of deformation on the magnetic properties of these alloys has not been extensively explored to date.

II. MATERIALS AND METHODS

CrMnFeCoNi and CrMnFeCoNi-CN samples were obtained from 5 kg ingots produced in a vacuum induction furnace in an argon atmosphere at 500 mbar, using as material premium pure components in their technical grade, in order to get closer to industry standards. Subsequently, a round bar was hot forged at 1323 K from an initial diameter of 42 to 12 mm, followed by solution annealing at the same temperature for 30 min and quenching in water.

The composition of the alloys is indicated in Table I. C and N were measured by carrier gas hot extraction (combustion method). The device for measuring C is a type CS-800 and for N a type ONH-2000 from company Eltra GmbH. Substitutional elements were measured by means of the EDS technique. For more details on the processing route and mechanical properties of the alloys investigated in this work, see Reference 16.

Following the DIN EN ISO 6892 standard, tensile tests were performed at $T = 298$ K in a Z100 Zwick universal test machine. At elongations of 10, 20, and 30 pct, deformation ceased. Materials that did not deform were saved for reference.

To determine the crystal structure of the alloys, X-ray diffraction (XRD) was performed at room temperature using a Panalytical X'pert PRO-MPD diffractometer with Ultra-fast X' Celerator detector and a Cu-Ka radiation source. Data were collected at 2θ with steps of 0.0263° every 100 s between 20 and 80 deg. Lattice parameters were obtained *via* refining with the PowderCell PCW23 software. A ZEISS EVO MA10 scanning electron microscope (SEM) was used to analyze microstructure of the alloys. For the SEM, conventional metallographic preparation consisting of grinding and polishing. Following, electrolytic etching with oxalic acid 10 pct and 2.5 V was applied. For this technique, the conditions were maintained during 90 s for the specimens in the non-deformed state, and for 60 s in the case of the deformed specimens.

Using a vibrating sample magnetometer (VSM) from Quantum Design, the magnetization as a function of applied field (M *vs* H) was measured at various temperatures 50 K, 100 K, 200 K, 250 K, and 300 K for each specimen, with deformations of 0, 10, and

20 pct. The same equipment is used to study magnetization as a function of temperature (M *vs* T), using the Zero Field Cooled (ZFC) and Field Cooled (FC) mode between 50 K and 370 K.

The ZFC test involves cooling the sample to 50 K in the absence of an applied magnetic field, then heating it to 370 K with an applied magnetic field (100Oe, 500Oe, 2000Oe, 5000Oe, 100000Oe, 25000Oe, and 30000Oe), while measuring the magnetic moment as a function of temperature. The FC test consists of measuring the magnetic moment as a function of temperature while cooling the sample from 370 K to 50 K with an applied magnetic field.

Magnetization as a function of temperature and external field curves were constructed using data obtained through the VSM technique. Equation [1] was utilized to compute magnetic susceptibility.

$$\chi = M/H, \qquad [1]$$

where M denotes the magnetization and H corresponds to the magnetic field strength. Additionally, inverse of magnetic susceptibility $\chi^{-1}(T)$ was plotted.

III. RESULTS

A. *Microstructure Analysis*

Figure 1 shows the microstructure of the equimolar CrFeMnCoNi and the CrMnFeCoNi-CN alloys at different degrees of deformation.

The micrographs correspond to the cross section of the specimens used for the tensile test; this means that the evaluated surface is perpendicular to the direction of load. In the initial state with no deformation, (Figures 1(a) and (d)) equiaxed homogeneous grains are observed, many of them contain annealing twins. The average grain size determined by a linear intercept method was 94 and 99 μm (twin boundaries were not counted in the measurements) for the CrMnFeMnCoNi and CrMnFeCoNi-CN alloys, respectively. In Figures 2(b), (c), (e), and (f) corresponding to 10 and 20 pct of deformation, a color contrast can be seen, corresponding to the variation in the intensity of backscattering observed with respect to changes in the orientation of the crystal. This contrast observed corresponds to the presence of grains with dislocation cells,

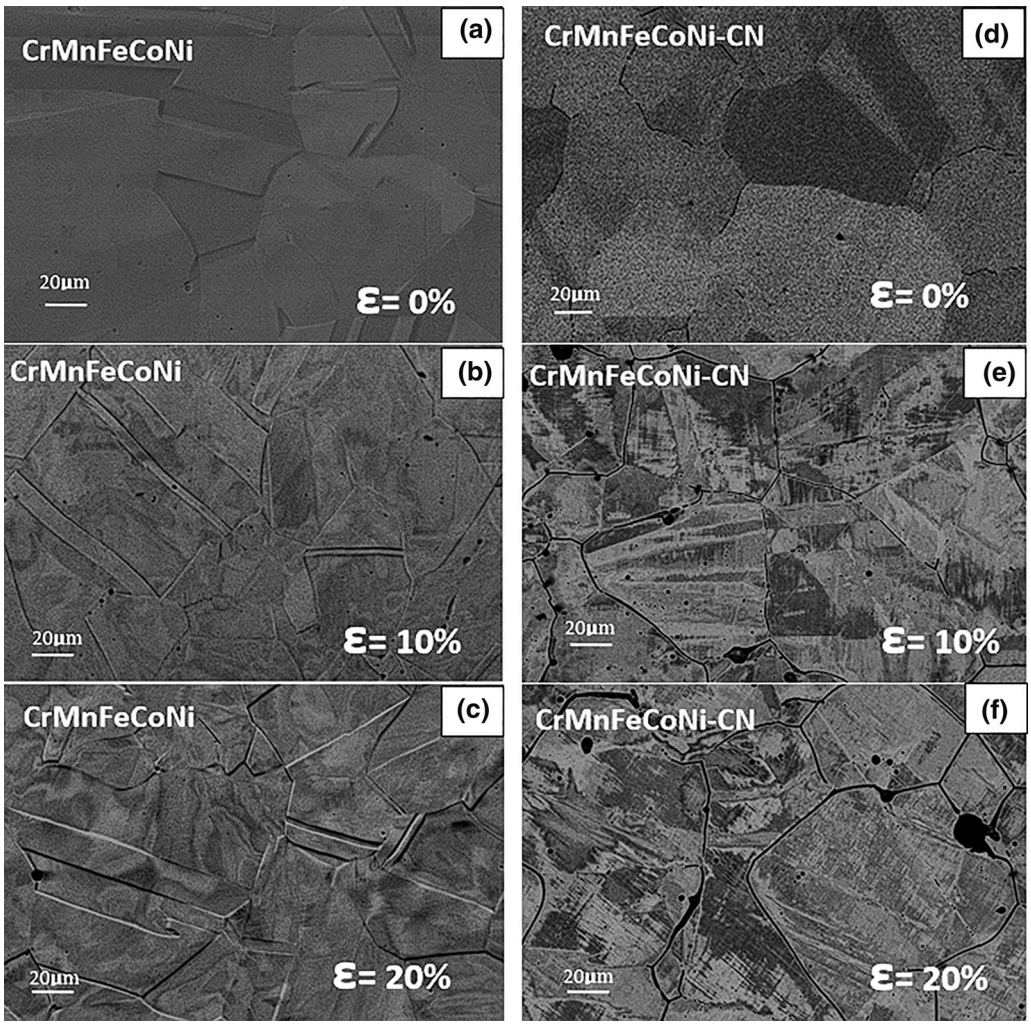

Fig. 1—SEM micrographs for CrMnFeCoNi and CrMnFeCoNi-CN alloys with strains of 0, 10, and 20 pct.

Table I. Composition of the Alloys (At. Pct)

Alloy	C	N	Co	Cr	Mn	Ni	Fe
CrMnFeCoNi	—	—	18.70	23.11	18.83	19.03	20.33
CrMnFeCoNi-CN	0.59 ± 0.03	0.31 ± 0.001	25.03	20.43	19.76	20.47	13.42

additionally, the wavy appearance of the contrast in some grains corresponds to the bending contours due to a change of orientation in the material.[44] Considering the stacking fault energy value for the CrMnFeCoNi alloy (30 ± 5 mJ/m^2),[45] it can be suggested that the main deformation mechanism at room temperature corresponds to dislocation slip, as previously reported.[45] For the CrMnFeCoNi-CN alloy, dislocation slip and twinning can be suggested as deformation mechanisms.

B. *XRD Analysis*

Figures 2(a) and (b) illustrate XRD analyses performed at room temperature. They show that a fcc single-phase solid solution crystal structure is present. In samples with 0, 10, and 20 pct of plastic deformation, the formation of α'-martensite or ε -martensite is not observed. The crystalline structure of the alloy, which corresponds to the space group Fm-3 m, was confirmed using the crystallographic file with code COD 1524833 as a reference. The diffraction pattern of the material displays the austenite planes (111) and (200) which are slightly shifted toward smaller angles with increasing deformation, showing an increase in the lattice parameter as a result of the deformation (Table II). Additionally, a broadening of the reflections is seen as deformation increases.

C. *Magnetic Response*

1. *CrMnFeCoNi alloy*

The reference CrMnFeCoNi material displays a paramagnetic behavior, a linear dependency of the magnetization on the applied external field, and a reduction in this with regard to the increase in temperature are observed (Figure 3). Additionally, an increment in magnetization is seen in the deformed samples, particularly at 10 pct deformation, indicating that the deformation in the material has an effect on the magnetic response.

An increase in magnetization with deformation caused by the external field is shown in the curves of magnetization as a function of temperature *M vs T* (Figure 4). The magnetization rose noticeably in the deformed samples; however, magnetization remains stable in the sample with a 20 pct of deformation compared to the 10 pct of deformation material. A reason for this behavior could be that at lower deformations, the strain-induced anisotropy in the material increases, which can enhance the alignment of magnetic moments and lead to higher magnetization. However, at higher deformations, this effect might saturate, leading

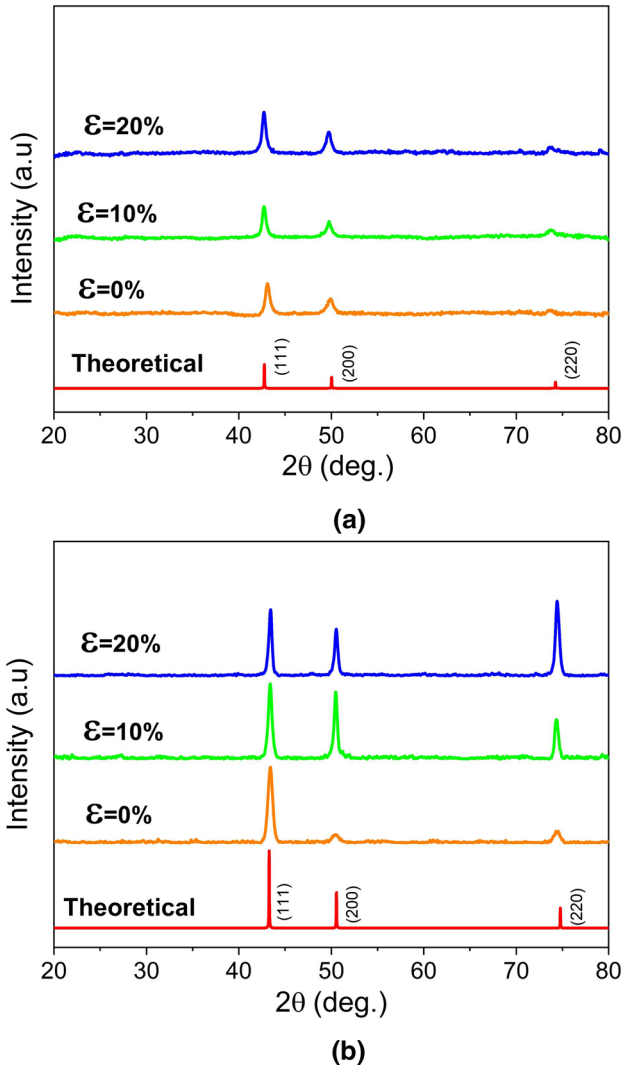

Fig. 2—(*a*) XRD pattern at different deformations for CrMnFeCoNi, (*b*) CrMnFeCoNi-CN.

Table II. Lattice Parameters Obtained for Each Value of Deformation

	Deformation (Pct ε)		
Alloy	0	10	20
CrMnFeCoNi	3.557(5)	3.595(6)	3.602(1)
CrMnFeCoNi-CN	3.606(2)	3.616(3)	3.624(5)

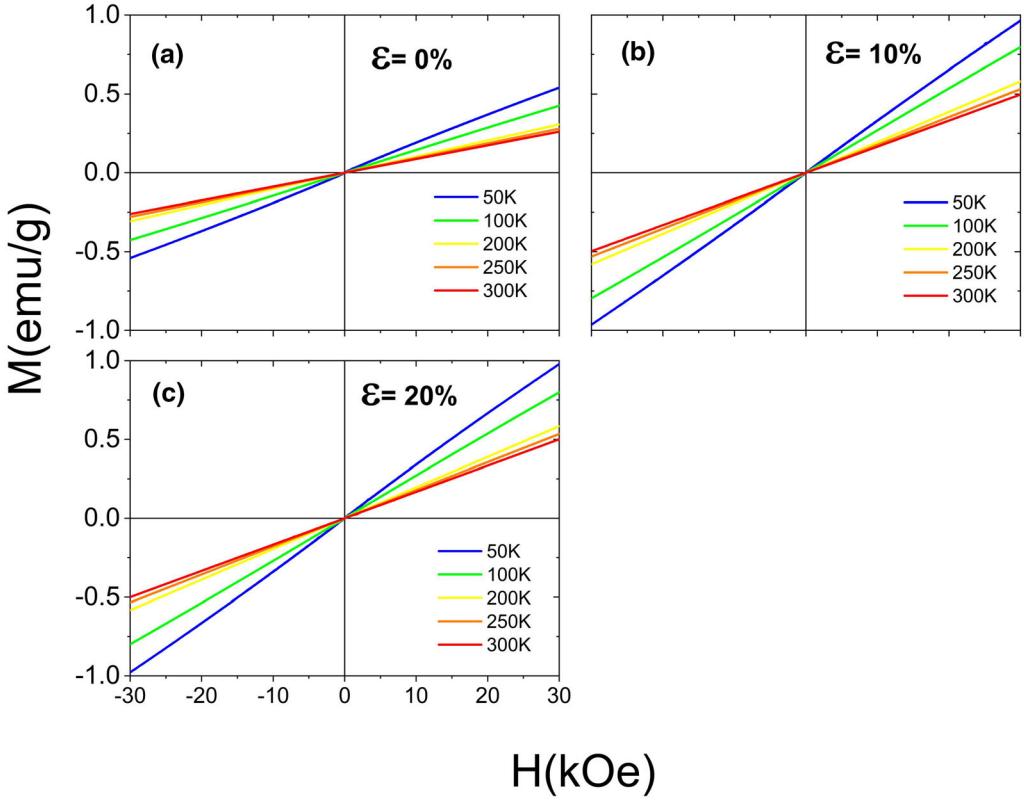

Fig. 3—Magnetization of CrMnFeCoNi alloy as a function of the external field at different values of deformation (*a*) 0 pct, (*b*) 10 pct, and (*c*) 20 pct.

to a plateau in magnetization. Additionally, from 0 to 10 pct deformation, the microstructure undergoes significant changes, leading to increased magnetic domains and hence higher magnetization. However, at higher levels of deformation like 20 pct, the microstructure may reach a more stable configuration, resulting in a stabilization of the magnetic response.

For the evaluated fields, magnetization values were obtained that fall within the range of values previously observed for high-entropy alloys, ranging from 0.0015 to 1.4 emu/g.[31,46–49] The magnetization was quantified in units of μB/f.u. (Bohr magneton/formula unit) and the formula unit (f.u.) is defined as $Fe_{0.20}Cr_{0.23}$ $Mn_{0.18}$ $Co_{0.18}$ $Ni_{0.19}$. For 50 K at a field of 30000 Oe, the magnetizations correspond to 0.0049, 0.009407, and 0.009603 μB/f.u for 0, 10, and 20 pct of deformation, respectively. These small magnetic moments appear to be smaller than the magnetic moments of the individual atoms that constitute the alloy reported in the literature (Table III). Since Mn and Cr make up 40 pct of the structure, a considerable reduction in the overall magnetic moment of the system is anticipated as a result of a high magnetic frustration caused by oscillations in these magnetic moments and by their antiferromagnetic coupling with Fe, Co, and Ni.[49]

For the sample without deformation, a clear deviation from the Curie-Weiss behavior at the so-called T_{ord} is observed (see Figure 5), which corresponds to 70 K and can be attributed to a slight magnetic ordering, this deviation is characterized by an inflection in the ideal curve.[31] On the other hand, this deviation is not observed in the deformed samples, indicating that the deformed state of the sample has an effect on the magnetic ground state of this group of materials. Additionally, an irreversibility in the magnetization is observed, that is, a separation of the ZFC and FC curves in the samples deformed at a temperature around 65 K indicated in the inset of Figure 5 as T_g. This irreversibility of the curves is more pronounced at lower deformations and could be attributed to possible spin glass behavior.[27,31,32]

The Curie–Weiss equation can be used to express the temperature dependence of the magnetic susceptibility in antiferromagnetic materials at temperature $T > T_{ord}$.

$$\chi(T) = C/(T + \theta_C), \qquad [2]$$

where θ is the Curie paramagnetic temperature and C is the Curie constant. Figure 6 shows the relationship between the reciprocal values of the magnetic susceptibility χ^{-1} and temperature. At a temperature below T = 250 K, the temperature dependence of χ^{-1} loses linearity. By extrapolating the linear portion of the χ^{-1} (T) dependency down to zero, it was determined that the values of the Curie temperatures (θ) are negative (Figure 5) (Table IV). Curie temperature (θ) describes the exchange interaction that still exists despite being suppressed by thermal motion. Negative values indicate the presence of antiferromagnetic interactions in the alloy. Additionally, Eq. [3] was used to

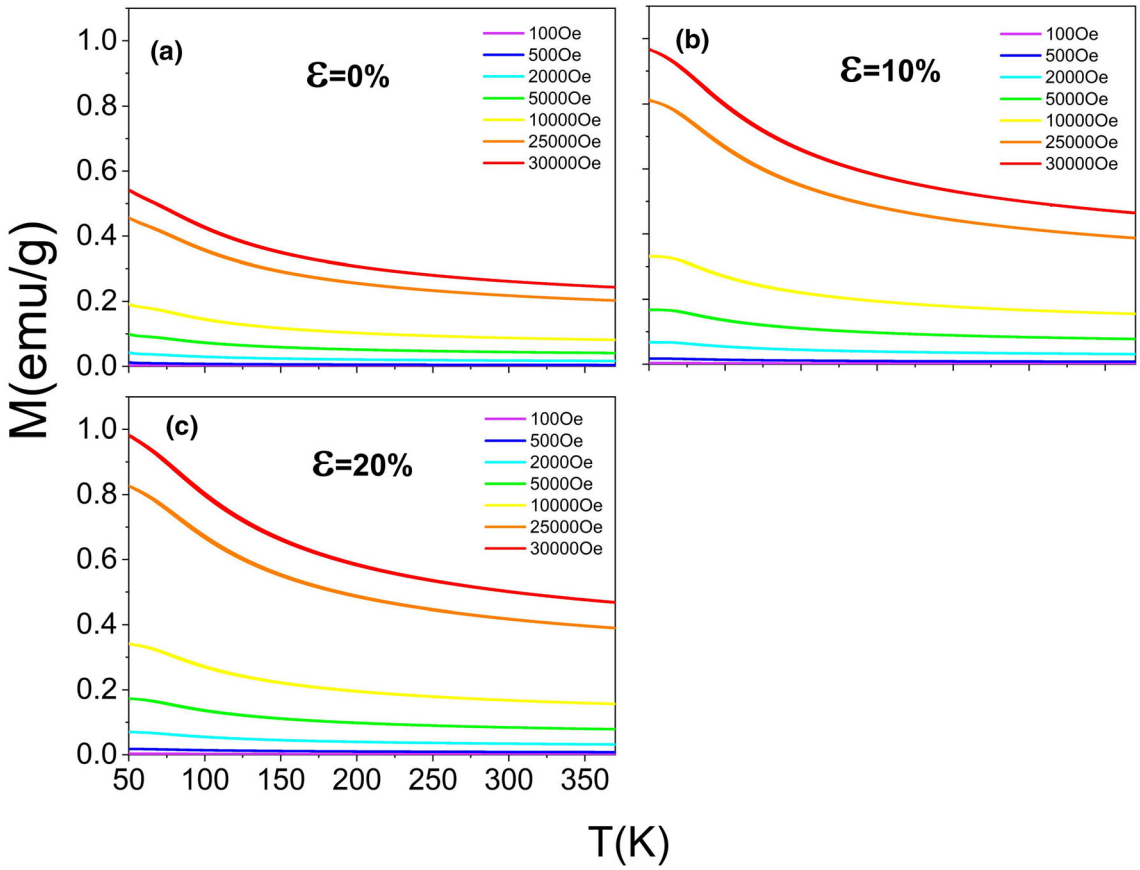

Fig. 4—Magnetization of CrMnFeCoNi alloy as a function of the temperature at different values of deformation (*a*) 0 pct, (*b*) 10 pct, and (*c*) 20 pct.

Table III. Magnetic Moments for Pure Elements: FM (Ferromagnetic), AFM (Antiferromagnetic)

Element	Structure	Magnetic Phase	Magnetic Moment (μB)	References
Cr	bcc	AFM	1.60	50
Mn	bcc	AFM	0.4 to 0.6	51
Fe	bcc	FM	2.15 to 2.26	52
Co	hcp	FM	0.87 to 2.83	53
Ni	fcc	FM	0.61t o 0.66	54

All values correspond to theoretical values.

determine the effective magnetic moment of the alloys (Table IV):

$$m_{eff}(\mu_B) = (3k_B * C_m/N_A)^{1/2}, \quad [3]$$

where k_B corresponds to Boltzmann constant, N_A denotes the Avogadro number, and C_m is the molar Curie units of emu-K/mol.

2. *CrMnFeCoNi-CN alloy*

CrMnFeCoNi-CN alloy has a linear dependency with no evidence of spontaneous magnetization and demonstrates a reduction in magnetization with respect to temperature. The paramagnetic behavior of the alloy can be inferred (Figure 7). The magnetization values do not change as the strain increases. Magnetization of all samples reaches a maximum of 1.25 emu/g at the evaluated temperatures.

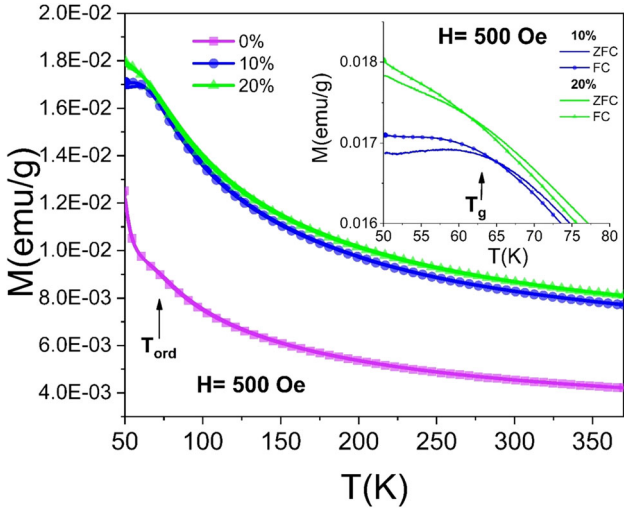

Fig. 5—Magnetization of CrMnFeCoNi alloy as a function of temperature for the CrMnFeCoNi alloy at an external field of 500Oe.

Additionally, the figures depicting of magnetization as a function of temperature (Figure 8) indicate an increase

in magnetization as a function of the applied external field, but without a change due to the deformation present in the material. This alloy does not show a deviation from Curie-Weiss behavior in the measured temperature range (see Figure 8).

A detailed analysis of the M vs T curves at 100 Oe shows an irreversibility or separation of the ZFC and FC curves at the so-called (T_g) (Figure 9). Interestingly, this phenomenon becomes negligible for all samples both deformed and undeformed at high external magnetic fields in the range of the measured temperature, indicating that the spin glass state will be gradually depressed with increasing applied magnetic field, and therefore, the ZFC and FC curves tend to coincide in high magnetic fields, and it is possible to suggest that the largest fields are sufficient to overcome the energy barrier between the disequilibrium configurations of the magnetic moments, this phenomenon is also observed in the CrMnFeCoNi alloy. However, it is suggested to evaluate this behavior in a lower temperature range.

The irreversibility could be attributed to magnetic coupling and the frustration that arises from the random distribution given by the presence of different magnetic states leading to the formation of glass-state magnetic arrangement at low temperatures. Likewise, it may be due to the anisotropy induced by the deformation in the material.

Figure 10 shows the curves corresponding to the magnetic susceptibility of the alloy to different degrees of deformation, obtaining a maximum value of 0.00315 emu/Oe-mol.

Taking the linear part of the inverse of the susceptibility as a function of the temperature, the Curie temperatures were estimated and effective paramagnetic moment was calculated for the three samples, finding the values described in Table V.

Curie temperatures have negative values as it can be seen in Figure 10(b) confirming the presence of local antiferromagnetic interactions within the alloy.

When five magnetic elements (Co, Fe, Ni, Cr, Mn) are randomly distributed in the lattice, the spin system adopts a configuration that is hindered or disrupted due to the preference for parallel spin alignment between Co, Fe, and Ni, and antiparallel spin alignment between Cr and Mn among their nearest neighbors. The high-entropy alloy CrMnFeCoNi-CN is a magnetically concentrated system that exhibits both randomness and frustration. Randomness refers to the fact that five different types of spins are randomly distributed throughout the lattice. Frustration arises because it is impossible to find a spin configuration that simultaneously satisfies all bonds and minimizes energy.

Table IV. Effective Magnetic Moment Values of CrMnFeCoNi Alloy at Different Deformations

Deformation (Pct ε)	Effective Magnetic Moment (μB)	Curie Temperature θ (K)
0	1.8117	− 526
10	2.5260	− 558
20	2.6001	− 547

IV. DISCUSSION

The complicated interactions between the constituent elements control the magnetization of an alloy. Three of the five components of the alloy (Fe, Co, and Ni) exhibit ferromagnetism. However, Mn and Cr exhibit an antiferromagnetic state with complex interactions, which modifies the magnetization of the alloy.[49] Due to the complex interactions between the constituent atoms, the overall magnetization is significantly reduced. This decrease in magnetism is attributed by Zhang *et al.*[47] to antiparallel alignment that causes magnetization cancelation. Additionally, Niu *et al.*[55] expected that the magnetic moments carried by Ni atoms would be significantly reduced, especially when combined with the L_{12}-type arrangement of Cr atoms.

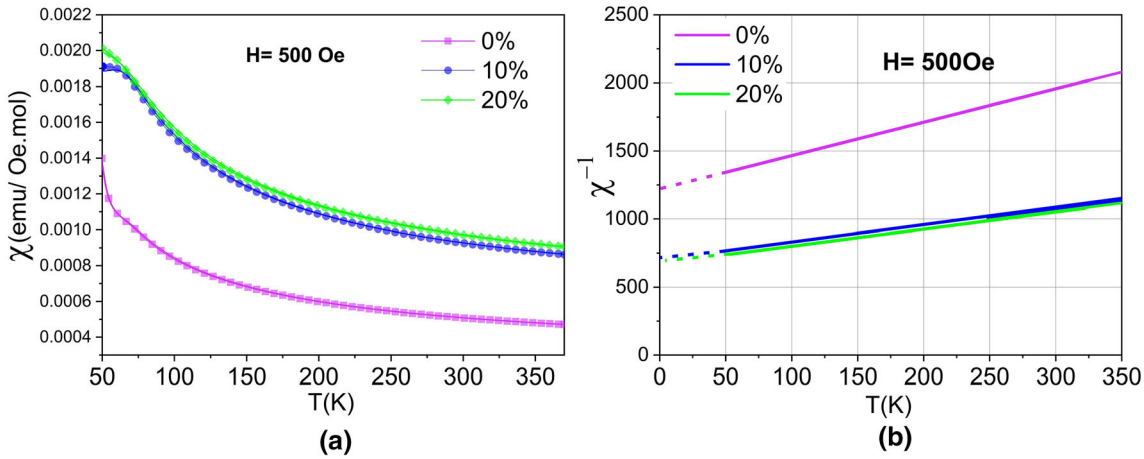

Fig. 6—(*a*) Magnetic susceptibility of CrMnFeCoNi alloy as a function of temperature, and (*b*) inverse of the magnetic susceptibility.

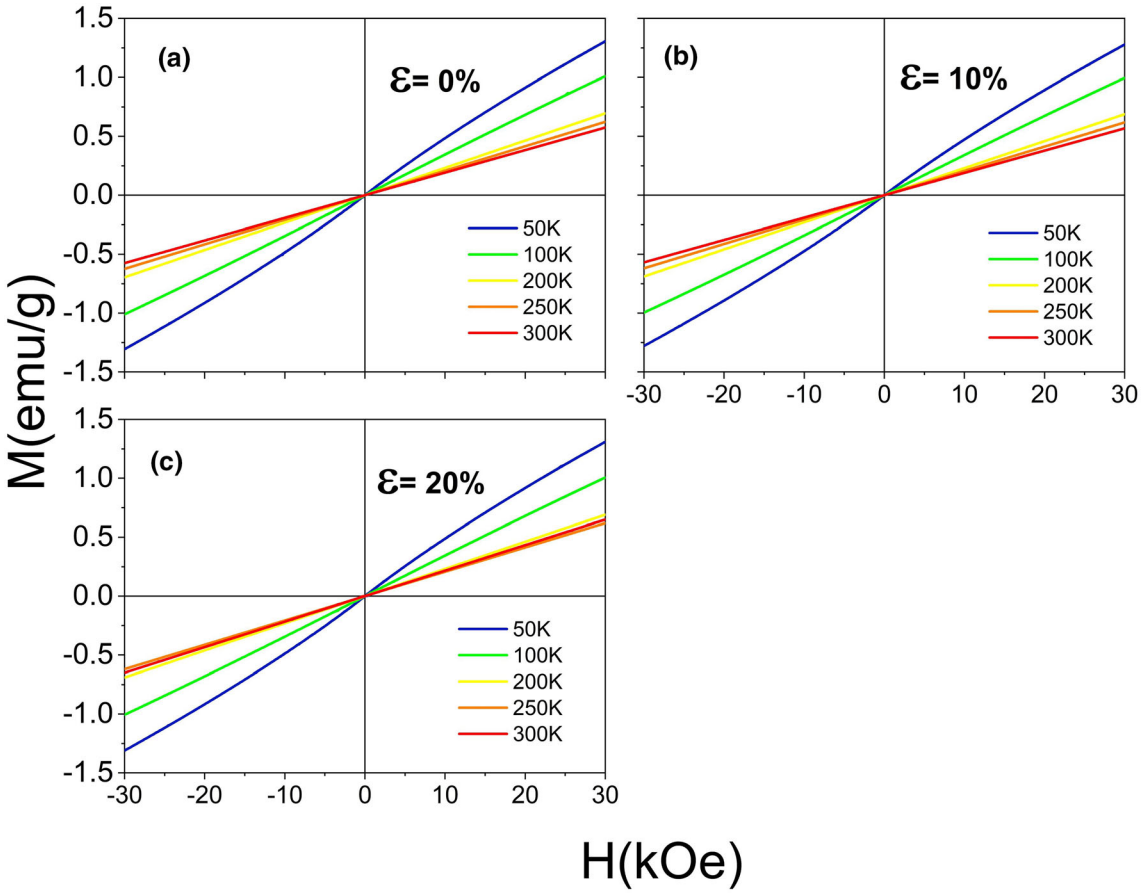

Fig. 7—Magnetization of CrMnFeCoNiCN alloy as a function of the external field at different values of deformation (*a*) 0 pct, (*b*) 10 pct, and (*c*) 20 pct.

The paramagnetic behavior of Cantor alloy at 300 K and the increase in magnetic moment linearly with applied magnetic field have been also confirmed in other studies.[29,30]

It is feasible to state that other factors, in addition to composition and crystalline structure, have a significant role in determining a certain magnetic property of the alloys.[56,57] Additionally, the mechanical deformation and heat treatment that the material has undergone must be taken into consideration.

Regarding the equimolar Cantor CrFeMnCoNi alloy, it was found that for a deformation of 0 pct, the material undergoes a slight magnetic ordering at a temperature of 70 K, which can be suggested as ferrimagnetism, a type of ordering where the populations of atoms with opposite magnetic moments (similar to antiferromagnetism) have unequal magnitudes, resulting in a small residual magnetization in the material. This ferrimagnetic ordering was previously reported by Kamarad *et al.*[31] at 85 K. Schneeweiss *et al.*[27] reported an ordering of the alloy to a ferromagnetic state at 38 K. DFT calculations performed by Elmslie *et al.*[58] showed two magnetic transitions of the Cantor alloy, one at 43 K and one at 85 K associated with a weak ferrimagnetic transition and a spin-glass-like transition, respectively.

For the samples with a degree of deformation, an increase in the magnetization of the material was observed, and a transition that can be attributed to a spin glass state or to an anisotropy induced by the deformation, this spin-glass-like behavior has been found in the Cantor alloy at 43.5 K[31] and 25 K.[32] The magnetic interactions between the atoms are closely related to the atomic environment; during the plastic deformation process, there are permanent changes in the atomic positions, which leads to a different interaction and magnetic coupling between the constituent atoms. The magnetization is locally driven in the preferred directions of magnetoelasticity due to the existence of dislocations. This has an effect both on the rotation of the magnetization in the direction of the magnetic field and on the movement of the walls of the magnetic domains.[59]

On the other hand, it has been shown that the magnetic ordering has an important influence on other properties of this type of alloys, such as the stacking fault energy. Niu *et al.*[60] report that for the CrCoNi system, which has better properties than the quinary alloy CrMnFeCoNi at room and cryogenic temperatures, the formation of a nanostructured hcp phase occurs caused by the metastability of the fcc phase at low temperatures, mechanism suppressed in the

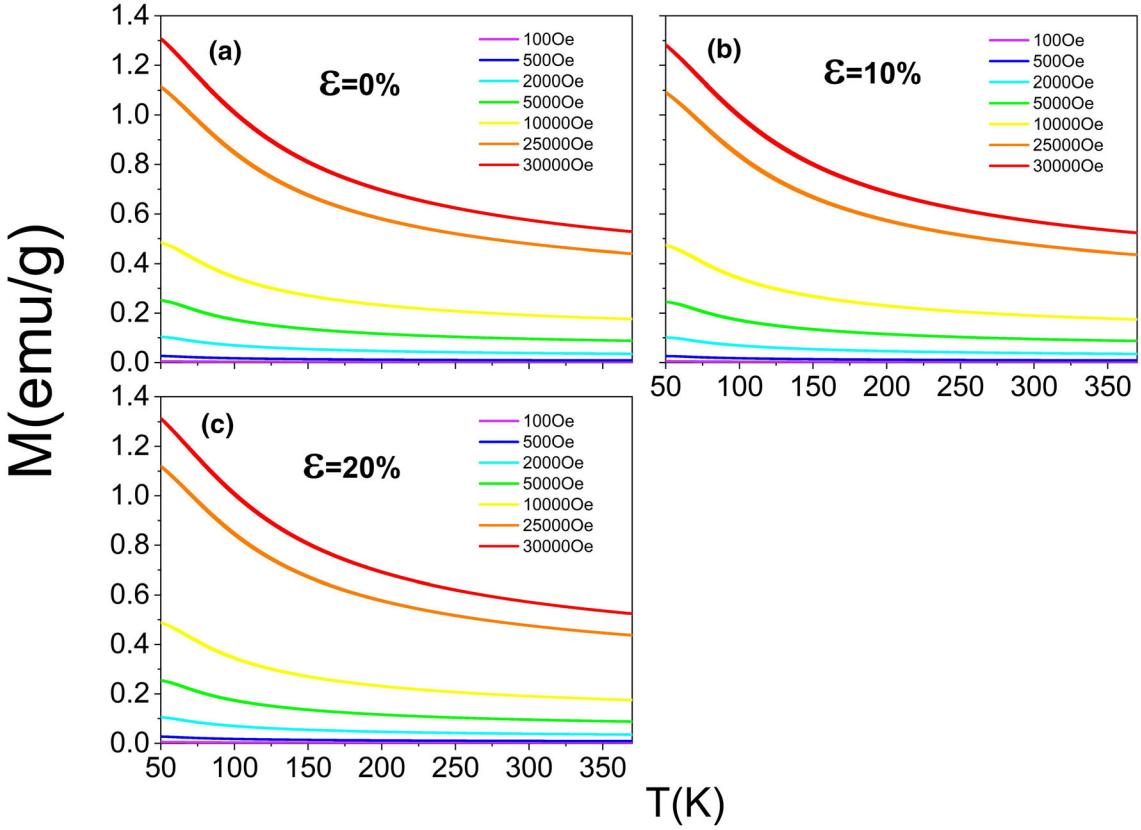

Fig. 8—Magnetization of CrMnFeCoNi-CN alloy as a function of the temperature at different values of deformation (*a*) 0 pct, (*b*) 10 pct, and (*c*) 20 pct.

CrMnFeCoNi alloy due to the existing magnetic frustration. Li *et al.*[61] through first principles calculations calculated the energy associated with four different single-phase fcc alloys considering the spin polarization, finding that the average energy of both the fcc and hcp phases is reduced considering magnetism. For Mn-containing alloys, magnetism has the greatest effect on the relative stability of the fcc and hcp phases.

For CrMnFeCoNi-CN alloy, it was observed that the magnetization of the alloy is susceptible to both the external field and the temperature. *M vs H* curves show a decrease in magnetization is evidenced with respect to the increase in temperature for the samples with 0, 10, and 20 pct deformation. Likewise, for *M vs T* curves, an increase in magnetization is observed as a function of the external field for all samples, both undeformed and undeformed.

For this alloy, it was observed that the magnetization is not strongly influenced by the deformation induced on the material, likewise the deformation mechanisms in the material can have an effect on the magnetic response of the material. One explanation to this could be that atomic environments of the material are not strongly influenced by the deformation process thus allowing the material to exhibit the same magnetic properties in its undeformed state as in its deformed state, in the range of deformation evaluated.

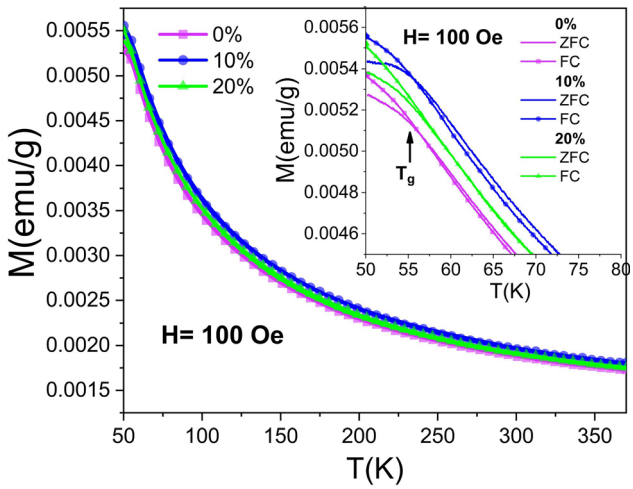

Fig. 9—Magnetization as a function of temperature for the CrMnFeCoNi-CN alloy at an external field of 100Oe.

The high-entropy CrMnFeCoNi-CN alloy contains elements with complex magnetic interactions, unlike the CrMnFeCoNi alloy, the CrMnFeCoNi-CN alloy did not present a slight ferrimagnetic ordering in the sample with 0 pct strain, this may be because the percentage of

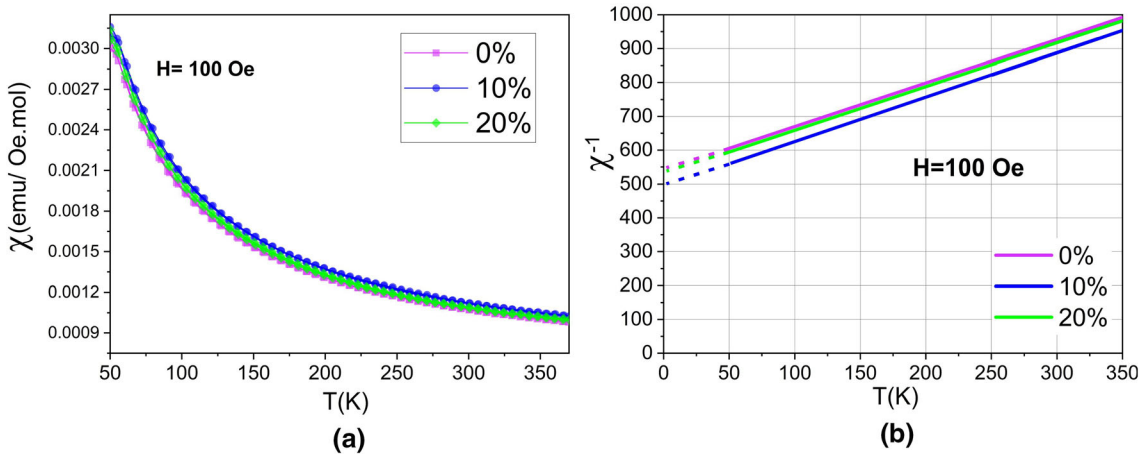

Fig. 10—(*a*) Magnetic susceptibility of CrMnFeCoNiCN alloy as a function of temperature, and (*b*) inverse of the magnetic susceptibility.

Table V. Effective Magnetic Moment Values of CrMnFeCoNi-CN Alloy at Different Deformations

Deformation (Pct ε)	Effective Magnetic Moment (μB)	Curie Temperature θ (K)
0	2.3878	− 448
10	2.3950	− 400
20	2.4797	− 420

the iron element is lower (13.75 wt pct), and therefore, there is a lower contribution to the ferromagnetic or ferrimagnetic ordering. Future work in order to discern whether Fe and Co substitutional contributions could be more representative compared with the effect of C and N on the lattice distortion and therefore on the magnetic response could be of interest.

Given the high magnetic frustration existing in the material, a transition from the paramagnetic state to the spin glass state is observed at temperatures of 55 K, 56, K and 54 K, for the samples with 0, 10, and 20 pct deformation, respectively. This transition as mentioned above takes place in magnetic systems characterized by disorder, where the competition between exchange interactions fails to produce a coherent alignment of magnetic moments over long distances. Instead, it results in a quasi-random immobilization of their distribution.

Regarding the influence of C and N on magnetic behavior, for some systems like Fe20Cr6Mn6CN, it has been shown that C and N slightly increase the magnetic moments,[62,63] in this case maximum magnetization value measured for the CrMnFeCoNi alloy was 1.0 emu/g in the evaluated range of temperature; meanwhile, 1.25 emu/g was the maximum magnetization value for CrMnFeCoNiCN supporting the idea that the addition of C and N increases magnetic moments to some extent. C and N atoms are dissolved in the octahedral interstices (O sites) of the supercell. There are two different positional relationships between the octahedral interstices: the first nearest neighbor and the second nearest neighbor. The atoms of C and N change the thermodynamic stability of the alloy, where the electronic transfer of metal atoms is sensitive to localized positions in the alloys, affecting the magnetic characteristics.[62,63]

The transition from paramagnetic to spin glass states in the CrMnFeCoNi-CN alloy highlights its potential in magnetic sensor technologies. Spin glass materials, known for their disordered magnetic states, are promising for sensing applications, such as in magnetic field sensors and spintronic devices. Additionally, the phase stability of these alloys makes them good candidates for structural components near high-field superconducting components, SQUID sensors, or electrical power generation rotors.

V. CONCLUSIONS

Both CrMnFeCoNi and CrMnFeCoNi-CN alloys have a homogeneous single fcc structure with no presence of secondary phases. Dislocation cells were identified in both alloys and twinning is suggested as deformation mechanism for CrMnFeCoNi-CN at room temperature.

Magnetization of the CrMnFeCoNi increases with deformation and external field and decreases with temperature. Small magnetic moments were found as expected due to the magnetic frustration of the constituent elements. For CrMnFeCoNi-CN, magnetization increases with external field and decreases with temperature, and important magnetic variations were not observed in the deformed samples with respect to the undeformed one.

Magnetic response as a function of temperature at a constant field shows that the unstrained CrMnFeCoNi alloy undergoes a slight ferrimagnetic ordering at about 70 K, and the strained samples have a transition to the spin glass state at about 63 K. The CrMnFeCoNi-CN alloy undergoes a transition to the spin glass state at a temperature of about 55 K in all samples both deformed and undeformed.

ACKNOWLEDGMENTS

L.G-Torres acknowledges the resources provided by UPTC under the convocation 19 of 2021, Project SGI 3282 and the Project UTM1999. L. Mujica, L.G. Torres and C. Parra acknowledge the support of the research center INCITEMA.

AUTHOR CONTRIBUTIONS

Conceptualization: L.G-T and L-M.R; methodology: C-P.V and L-M.R; validation: S-W, J-L, and L-M.R; formal analysis: L.G-T and L-M.R; resources: C-P.V, S-W, J-L, and L-M.R; and writing-original draft preparation: L.G-T. All authors have read and agreed to the published version of the manuscript.

FUNDING

Open access funding provided by Colombia Consortium.

CONFLICT OF INTEREST

The authors declare that they have no known competition financial interest or personal relationship that could have appeared to influence the work reported in this paper.

REFERENCES

1. A. Gali and E.P. George: *Intermetallics (Barking)*, 2013, vol. 39, pp. 74–78.
2. J. Chen, X. Zhou, W. Wang, B. Liu, Y. Lv, W. Yang, D. Xu, and Y. Liu: *J. Alloys Compd.*, 2018, vol. 760, pp. 15–30.
3. Y. Shi, Y.D. Wang, S. Li, R. Li, and Y. Wang: *Mater. Sci. Eng. A. Sci. Eng. A*, 2020, vol. 788, pp. 1–9. https://doi.org/10.1016/j.msea.2020.139600.
4. J.W. Yeh: *JOM*, 2015, vol. 67, pp. 2254–61.
5. P.K.L.J. Brechtl: *High-Entropy Materials: Theory, Experiments, and Applications*, 1st ed. Springer, Cham, 2022, pp. 1–62.
6. H. Liu, H. Qin, J. Kang, L. Ma, G. Chen, Q. Huang, Z. Zhang, E. Liu, H. Lu, J. Li, and N. Zhao: *Chem. Eng. J.*, 2022, vol. 435, 134898https://doi.org/10.1016/j.cej.2022.134898.
7. Z. Zhang, J. Hu, B. Li, Q. Qi, Y. Zhang, J. Chen, P. Dong, C. Zhang, Y. Zhang, and M.K.H. Leung: *J. Alloys Compd.*, 2022, vol. 918, 165585https://doi.org/10.1016/j.jallcom.2022.165585.
8. B. Wang, Y. Yao, X. Yu, C. Wang, C. Wu, and Z. Zou: *J. Mater. Chem. A*, 2021, vol. 9, pp. 19410–38.
9. S. Schumacher, S. Baha, A. Savan, C. Andronescu, and A. Ludwig: *J. Mater. Chem. A*, 2022, https://doi.org/10.1039/D2TA01652D.
10. Y. Xin, S. Li, Y. Qian, W. Zhu, H. Yuan, P. Jiang, R. Guo, and L. Wang: *ACS Catal.Catal.*, 2020, vol. 10, pp. 11280–1306.
11. F. Yang, J. Wang, Y. Zhang, Z. Wu, Z. Zhang, F. Zhao, J. Huot, J.G. Novaković, and N. Novaković: *Int. J. Hydrogen Energy. J. Hydrogen Energy*, 2022, vol. 47, pp. 11236–49.
12. X. Wang, W. Guo, and Y. Fu: *J. Mater. Chem. A Mater*, 2021, vol. 9, pp. 663–701.
13. S. Huang, W. Li, X. Li, S. Schönecker, L. Bergqvist, E. Holmström, L.K. Varga, and L. Vitos: *Mater. Des.*, 2016, vol. 103, pp. 71–74.
14. T. Zuo, X. Yang, P.K. Liaw, and Y. Zhang: *Intermetallics (Barking)*, 2015, vol. 67, pp. 171–76.
15. T. Zuo, M.C. Gao, L. Ouyang, X. Yang, Y. Cheng, R. Feng, S. Chen, P.K. Liaw, J.A. Hawk, and Y. Zhang: *Acta Mater. Mater.*, 2017, vol. 130, pp. 10–18.
16. L. Chmielak, L.M. Roncery, P. Niederhofer, S. Weber, and W. Theisen: *SN Appl. Sci.*, 2021, vol. 3, p. 835. https://doi.org/10.1007/s42452-021-04814-y.
17. J.Y. Aguilar-Hurtado, A. Vargas-Uscategui, K. Paredes-Gil, R. Palma-Hillerns, M.J. Tobar, and J.M. Amado: *Appl. Surf. Sci.*, 2020, vol. 515, 146084.
18. F. Otto, A. Dlouhý, C. Somsen, H. Bei, G. Eggeler, and E.P. George: *Acta Mater. Mater.*, 2013, vol. 61, pp. 5743–55.
19. M.C. Gao, J.-W. Yeh, P.K. Liaw, and Y. Zhang: *High-Entropy Alloys*, Springer, Cham, 2016.
20. B. Cantor, I.T.H. Chang, P. Knight, and A.J.B. Vincent: *Mater. Sci. Eng. A*, 2004, vol. 375–377, pp. 213–18.
21. P. Sathiyamoorthi and H.S. Kim: *Prog. Mater. Sci.. Mater. Sci.*, 2022, vol. 123, 100709.
22. B. Gludovatz, E.P. George, and R.O. Ritchie: *JOM*, 2015, vol. 67, pp. 2262–70.
23. G. Laplanche, A. Kostka, O.M. Horst, G. Eggeler, and E.P. George: *Acta Mater. Mater.*, 2016, vol. 118, pp. 152–63.
24. J.X. Fang, J.X. Wang, Y.J. Wang, H.T. He, D.B. Zhang, and Y. Cao: *Mater. Sci. Eng. A*, 2022, vol. 847, 143319.
25. R. Kozak, A. Sologubenko, and W. Steurer: *Zeitsch. Kristallogr.*, 2015, vol. 230, pp. 55–68.
26. J.W. Yeh, S.K. Chen, S.J. Lin, J.Y. Gan, T.S. Chin, T.T. Shun, C.H. Tsau, and S.Y. Chang: *Adv. Eng. Mater.*, 2004, vol. 6, pp. 299–303.
27. O. Schneeweiss, M. Friák, M. Dudová, D. Holec, M. Šob, D. Kriegner, V. Holý, P. Beran, E.P. George, J. Neugebauer, and A. Dlouhý: *Phys. Rev. B*, 2021, vol. 96, 014437https://doi.org/10.1103/PhysRevB.96.014437.
28. P.F. Yu, L.J. Zhang, H. Cheng, H. Zhang, M.Z. Ma, Y.C. Li, G. Li, P.K. Liaw, and R.P. Liu: *Intermetallics (Barking)*, 2016, vol. 70, pp. 82–87.
29. Y.Y. Tan, Z.J. Chen, M.Y. Su, G. Ding, M.Q. Jiang, Z.C. Xie, Y. Gong, T. Wu, Z.H. Wu, H.Y. Wang, and L.H. Dai: *J. Mater. Sci. Technol.*, 2022, vol. 104, pp. 236–43.
30. Y.Y. Tan, M.Y. Su, Z.C. Xie, Z.J. Chen, Y. Gong, L.R. Zheng, Z. Shi, G. Mo, Y. Li, L.W. Li, H.Y. Wang, and L.H. Dai: *Intermetallics (Barking)*, 2021, vol. 129, 107050.
31. J. Kamarád, M. Friák, J. Kaštil, O. Schneeweiss, M. Šob, and A. Dlouhý: *J. Magn. Magn. Mater.Magn. Magn. Mater.*, 2019, vol. 487, 165333https://doi.org/10.1016/j.jmmm.2019.165333.
32. M.H. Tsai: *Entropy*, 2013, vol. 15, pp. 5338–45.
33. X. Wu, Z. Li, Z. Rao, Y. Ikeda, B. Dutta, F. Körmann, J. Neugebauer, and D. Raabe: *Phys. Rev. Mater.*, 2020, https://doi.org/10.1103/PhysRevMaterials.4.033601.
34. W. Łoński, M. Spilka, M. Kądziołka-Gaweł, P. Gębara, A. Radoń, T. Warski, S. Łoński, K. Barbusiński, K. Młynarek-Zak, and R. Babilas: *J. Alloys Compd.*, 2023, vol. 934, 167827.

35. R. Babilas, W. Łoński, P. Boryło, M. Kądziołka-Gaweł, P. Gębara, and A. Radoń: *J. Magn. Magn. Mater.Magn. Magn. Mater.*, 2020, vol. 502, 166492.
36. P. Kumari, A.K. Gupta, R.K. Mishra, M.S. Ahmad, and R.R. Shahi: *J. Magn. Magn. Mater.Magn. Magn. Mater.*, 2022, vol. 554, 169142.
37. W. Łoński, M. Spilka, M. Kądziołka-Gaweł, P. Gębara, A. Radoń, T. Warski, K. Młynarek-Żak, and R. Babilas: *J. Alloys Compd.*, 2022, vol. 905, 164074.
38. Z. Li, J. Qi, Z. Li, H. Li, H. Xu, G. Bai, X. Liu, and X. Zhang: *Mater. Lett.Lett.*, 2021, vol. 297, 129965.
39. M. Földeáki, H. Ledbetter, and P. Uggowitzer: *J. Magn. Magn. Mater.Magn. Magn. Mater.*, 1992, vol. 110, pp. 185–96.
40. L.G. Torres-Mejía, K. Paredes-Gil, C.A. Parra Vargas, J. Lentz, S. Weber, and L. Mujica-Roncery: *Metall. Mater. Trans. A*, 2024, vol. 55, pp. 150–60.
41. N. Shkodich, F. Staab, M. Spasova, K.V. Kuskov, K. Durst, and M. Farle: *Materials*, 2022, vol. 15, p. 7214. https://doi.org/10.3390/ma15207214.
42. S. Uporov, V. Bykov, S. Pryanichnikov, A. Shubin, and N. Uporova: *Intermetallics (Barking)*, 2017, vol. 83, pp. 1–8.
43. G. Hausch: *J. Phys. Soc. Jpn.Jpn.*, 1974, vol. 37, pp. 819–23.
44. S. Zaefferer and N.N. Elhami: *Acta Mater. Mater.*, 2014, vol. 75, pp. 20–50.
45. E.P. George, D. Raabe, and R.O. Ritchie: *Nat. Rev. Mater.*, 2019, vol. 4, pp. 515–34.
46. D. Ma, B. Grabowski, F. Körmann, J. Neugebauer, and D. Raabe: *Acta Mater. Mater.*, 2015, vol. 100, pp. 90–97.
47. Y. Zhang, T. Zuo, Y. Cheng, and P.K. Liaw: *Sci. Rep.*, 2013, vol. 3, p. 1455. https://doi.org/10.1038/srep01455.
48. K. Perzyńska, A. Go, K. Szymański, M. Biernacka, Hawełek, B. Kalska-Szostko, D. Oleszak, K. Rećko, J. Waliszewski, and P. Zaleski: in *Proceedings of the 8th International Conference on Mechanochemistry and Mechanical Alloying, INCOME 2014*, Polish Academy of Sciences, 2014, pp. 999–1004.
49. M. Egilmez and W. Abuzaid: *Sci. Rep.*, 2021, vol. 11, p. 8048. https://doi.org/10.1038/s41598-021-87527-x.
50. E. Fawcett: *Rev. Mod. Phys.*, 1988, vol. 60, pp. 209–83. https://doi.org/10.1103/RevModPhys.60.209.
51. D. Hobbs, J. Hafner, and D. Spišák: *Phys. Rev. B. Rev. B*, 2003, vol. 68, p. 014407. https://doi.org/10.1103/PhysRevB.68.014407.
52. S. Yang, Y. Wang, Z.-K. Liu, and Y. Zhong: *Comput. Mater. Sci.. Mater. Sci.*, 2023. https://doi.org/10.1016/j.commatsci.2023.112299.
53. W. Betteridge: *Prog. Mater. Sci.. Mater. Sci.*, 1980, vol. 24, pp. 51–142.
54. S.E. Apsel, J.W. Emmert, J. Deng, and L.A. Bloomfield: *Phys. Rev. Lett.Lett.*, 1996, vol. 76, p. 1441. https://doi.org/10.1103/PhysRevLett.76.1441.
55. C. Niu, A.J. Zaddach, A.A. Oni, X. Sang, J.W. Hurt, J.M. Lebeau, C.C. Koch, and D.L. Irving: *Appl. Phys. Lett.Lett.*, 1906, vol. 2015, p. 16. https://doi.org/10.1063/1.4918996.
56. Z. Dong and L. Vitos: *Scr. Mater.*, 2019, vol. 171, pp. 78–82.
57. S. Huang, E. Holmström, O. Eriksson, and L. Vitos: *Intermetallics (Barking)*, 2018, vol. 95, pp. 80–84.
58. T.A. Elmslie, J. Startt, S. Soto-Medina, Y. Yang, K. Feng, R.E. Baumbach, E. Zappala, G.D. Morris, B.A. Frandsen, M.W. Meisel, M.V. Manuel, R. Dingreville, and J.J. Hamlin: *Phys. Rev. B*, 2022, vol. 106, p. 014418. https://doi.org/10.1103/PhysRevB.106.014418.
59. A. Seeger: *J. Phys. Colloques*, 1966, vol. 27, pp. 68–77. https://doi.org/10.1051/jphyscol:1966308.
60. A.J. Zaddach, C. Niu, C.C. Koch, and D.L. Irving: *JOM*, 2013, vol. 65, pp. 1780–89.
61. S.F. Liu, Y. Wu, H.T. Wang, J.Y. He, J.B. Liu, C.X. Chen, X.J. Liu, H. Wang, and Z.P. Lu: *Intermetallics (Barking)*, 2018, vol. 93, pp. 269–723.
62. Z. Lv, T. Liu, Z. Wu, K. Guan, and Y. Li: *J. Magn. Magn. Mater.Magn. Magn. Mater.*, 2020, vol. 504, p. 166663. https://doi.org/10.1016/j.jmmm.2020.166663.
63. Z. Lv, Q. Zhang, R. Li, Y. Hong, and X. Zhang: *J. Mater. Eng. Perform.*, 2021, vol. 30, pp. 8322–35.